의학석사 학위논문

Quantitative Assessment of Vascular Permeability in Migraine on Dynamic Contrast-Enhanced Magnetic Resonance Imaging

동적 조영 증강 자기 공명 영상에서 편두통의 혈관 투과성에 대한 정량 분석

2019 년 02 월

서울대학교 대학원

의학과 영상의학 전공

김 연 수

Abstract

Quantitative Assessment of Vascular Permeability in Migraine on Dynamic Contrast-Enhanced Magnetic Resonance Imaging

Yeon Soo Kim

Department of Radiology, College of Medicine

The Graduate School

Seoul National University

Introduction: To determine the pathophysiologic loci of migraine, we analyzed the quantitative blood-brain-barrier (BBB) permeability in migraine-associated brain regions using dynamic contrast-enhanced (DCE) magnetic resonance imaging (MRI).

Materials and methods: From September 2016 to December 2017, 56 subjects underwent DCE MRI after gadobutrol administration and were classified into migraine (n=35) and control groups (n=21). Automatic volumetric segmentation was performed on the precontrast T1-weighted image using FreeSurfer, and migraine-

associated brain region masks were extracted using NordicICE. The corresponding pharmacokinetic parameters of K_{trans}, the volume transfer constant, and V_p, the fractional plasma volume, maps were coregistered with the region of interest masks, and their statistics were calculated. For comparison between the two groups, the unpaired t-test or Mann-Whitney test was used. Receiver operating characteristic curve analysis and logistic regression analysis were used to identify correlations between clinical characteristics and the aforementioned perfusion parameters.

Results: Age in the migraine group was significantly younger than that in the control group ($p<0.0001$). In the migraine group, the mean value of V_p in the left amygdala was lower than those in the control group ($p=0.0382$). Only the mean value of V_p in the left amygdala had a correlation with the intensity of headache attack in migraine patients ($p=0.0350$).

Conclusion: The decreased V_p in the left amygdala is related to migraine, which can be used as a migraine-associated imaging biomarker.

Keywords: Migraine, Dynamic contrast-enhanced magnetic resonance imaging, Blood-brain-barrier, Permeability

Student Number: 2017-27607

Table of contents

List of tables

List of figures

Introduction

Migraine is a neurovascular disorder characterized by recurrent headache, associated with temporary autonomic nervous system dysfunction.(1) Previous studies have described structural and functional brain changes as a result of migraine attacks: enhanced cortical excitability(2, 3); gray matter volume change in some regions(4); and altered functional connectivity between the pain modulatory and the limbic system.(5, 6) Among those changes, the blood-brain-barrier (BBB) disruption and its sterile inflammation are important contributors to the migraine.(7, 8)

Dynamic contrast-enhanced (DCE) magnetic resonance imaging (MRI) requires the serial acquisition of images after intravenous contrast injection.(9) As a T1-shortening effect of gadolinium-based magnetic resonance contrast is maintained when extravasated into the interstitial space(8, 10), DCE MRI using the T1-shortening effect can determine the microcirculation permeability and measure the degree of signal enhancement reflecting the perfusion and permeability properties of tissue.(10, 11)

Recent studies have raised the possibility that BBB permeability might be associated with chronic pain.(12) The inflammatory pain produces structural changes in the major efflux transporter at the BBB and could lead to changes in the brain endothelial permeability.(12) Although measurement of BBB breakdown remains challenging because of a lack of fast imaging techniques(13-15), objective measuring and imaging parameter modeling(16), it would be a valuable aid in the diagnosis and measurement of the therapeutic response in neurovascular disorders.(15) However, there have been no evaluations of BBB permeability evaluation in migraine by using DCE MRI. Increased BBB permeability might suggest the pathophysiologic loci of brain in migraine. Thus, the purpose of this study is to measure the quantitative BBB permeability in migraine-associated brain regions using DCE MRI.

Materials and methods

Standard protocol approvals

This prospective study was approved by our institutional review board and a health care proxy for each patient provided written informed consent.

Patient population

From September 2016 to December 2017, we recruited a MRI-BBB cohort of subjects with headache who needed further brain MRI examination to evaluate the BBB permeability and identified 151 consecutive participants from the cohort (41 men and 110 women; mean age ± standard deviation (SD): 63.20 ± 12.87 years; age range, 26-87 years). Of 151 participants, 95 were excluded for the following reasons: (a) clinically uncertain diagnosis of migraine (n=14); (b) other disease entities, such as cluster headache, tension-type headache, and aneurysm, that may present similar symptoms to migraine (n=31); (c) inadequate image for DCE analysis because of severe internal cerebral artery stenosis or

irregularity (n=4); (d) inadequate image for control group because of moderate to severe small-vessel disease (n=13); (e) suboptimal image quality for DCE analysis because of severe motion artifact (n=24); and (f) patients who refused to participate in this study (n=9). The inclusion criteria were as follows: (a) absence of other lesions, except for the small unidentified bright objects and (b) conventional MRI with DCE MRI available for total volume analysis. Finally, 56 participants from the MRI-BBB cohort were included in this study population (14 men and 42 women; mean age ± SD: 61.17 ± 14.64 years; age range, 26-87 years) and were divided into the migraine (n=35) and control groups (n=21) (Figure 1). The patients of the migraine group were assigned to the low-frequency (LF) and high-frequency (HF) subgroups based on the frequency of headache attack per month. The former group (68.57%, 24/35) was defined as having 14 or fewer per month and the latter (31.43%, 11/35) at least 15 per month.(17)

The final migraine diagnosis was made by an experienced neurologist (M.H.K.) on clinical grounds based on the International Headache Society criteria. All the migraine patients fulfilled the

International Headache Society classification criteria of migraine with typical aura or without aura.(1) All 35 migraine patients underwent MRI during the interictal phase.

Clinical characteristics in each migraine patient were evaluated by an experienced neurologist (M.H.K) and the others were contacted by one of the investigators by phone to review their clinical characteristics.

Imaging protocol

All patients underwent DCE MRI studies with a 3-T imaging unit with a 32-channel head coil (Discovery 750; GE Healthcare, Milwaukee, Wisconsin). The MRI protocol included pre- and postcontrast three-dimensional fast spoiled gradient echo sequences with multiplanar reconstructions in the sagittal, coronal, and transverse T1-weighted image (T1WI) (Supplementary Table 1).

The specific parameters for the sequences were as follows: sagittal T1WI and reconstructed transverse and coronal images acquired before and after contrast enhancement with a 3D rapid acquisition of the gradient-echo sequence. For the gradient-echo

sequence, the following magnetic resonance parameters were used: repetition time, 8.5 ms; echo time, 3.2 ms; flip angle, 12° ; and matrix 256 x 230 with a section thickness of 1mm, a field of view of 256 x 256, and 1 acquired signal. Contrast-enhanced imaging was performed after intravenous administration of gadobutrol (Gadovist, Bayer Schering Pharma, Berlin, Germany) at a dose of 0.1 mml/L per kilogram of body weight. DCE MRI was performed by using 3D gradient-echo T1WI after intravenous administration of gadobutrol (0.1 mml/L/kg) by using a power injector (Spectris, MedRad, Indianola, Pennsylvania) at a rate of 4 mL/s. A 30-mL bolus injection of saline followed gadobutrol treatment at the same injection rate. For each section, 40 images were acquired at intervals equal to the repetition time. The following magnetic resonance parameters were used: repetition time, 3.0 ms; echo time, 1.1 ms; flip angle, 10° ; and matrix, 128 x 128 with a section thickness of 3mm, an field of view of 249 x 249mm, a voxel size of 1.25 x 1.25 x 3 mm^3, a pixel bandwidth of 789 Hz, and a total acquisition time of 5 minutes 25 seconds.

MRI analysis

Image analysis

All image analyses were performed by one radiologist (Y.S.K. with 3 years of brain MRI experience), who was supervised by an expert neuroradiologist (S.H.C. with 17 years of experience in neuroradiology), as described below.

Automatic cortical reconstruction and volumetric segmentation were performed on the precontrast T1WI using the default settings of the software for the analysis and visualization of structural neuroimaging data (FreeSurfer ver. 6.0; Laboratory for Computational Neuroimaging, Boston, MA, USA) (Figure 2). The following processes were done using FreeSurfer software(18): motion correction and averaging(19) of multiple volumetric T1WIs; removal of nonbrain tissue using a hybrid watershed/surface deformation procedure; segmentation of the subcortical white matter and deep gray matter volumetric structures; intensity normalization(20); tessellation of the gray matter–white matter boundaries; automated topology correction(21); surface deformation(22); and registration of the subjects' brains to a

common spherical atlas.(17) One radiologist (Y.S.K.) examined individual images for potential defects of reconstruction.

The following masks were selected according to the interested brain regions which are reported to be correlated with the migraine (Supplementary Table 2). All of the masks except for the brainstem had 3 masks: bilateral hemispheres; right hemisphere; left hemisphere. The total of 46 masks of brain regions of interest related to the migraine were obtained.

DCE MRI data were processed by using dedicated commercial software package (NordicICE; version 2.3.12; NordicNeuroLab, Bergen, Norway). For each patient, the arterial input function (AIF) was obtained from DCE MRI data with the DCE module in the software (NordicICE). After the data were loaded, motion correction and noise modulation were performed. An automatic detection method was used with an AIF searching box at the level of the middle cerebral artery horizontal segment. The final AIF was the mean of the five to six different AIFs from five to six pixels, which were automatically adopted on the basis of the cluster analysis technique.

Based on automatic method, the AIFs were obtained by analyzing all pixel-time curves in the dataset and applying cluster analysis to select the time courses that most resembled the expected input function properties, satisfying large area under the curve, low first moment, and high peak enhancement. (23, 24) All of the pharmacokinetic (PK) parameter maps were obtained using the AIF (Figure 3).(8)

The PK DCE parameters, including K_{trans}, the volume transfer constant for gadolinium between blood plasma and the tissue extravascular extracellular space, and V_p, the fraction plasma volume, maps, were obtained based on a two-compartment PK model using the Patlak graphical approach(25, 26), which is the most appropriate model in a low-leakage regimen.(2, 15, 27) Each parameter was calculated by using the fixed T1 of 1000 ms.(3, 23) Finally, K_{trans} and V_p maps were obtained in each subject.

Coregistration between the previously obtained interested brain region masks and the parameter maps from DCE MRI was automatically performed by an algorithm that found the most

appropriate transformation, based on the geometric information stored in the respective data set.(6, 8)

Ninety-two coregistration images in each patient were obtained by coregistration between 46 automatically reconstructed mask images and K_{trans} and V_p perfusion maps based on geometric information stored in the respective data sets with the software (NordicICE).(4) The differences in the slice thickness between images were automatically corrected by reslicing and coregistration based on the underlay and structural images. The automatic segmented masks were displayed as color overlays on the K_{trans} and V_p maps, respectively. The total volume of interest (VOI) in each section were determined by the automatic segmented mask.

On every axial image, PK parameters were calculated for the mask on a pixel-by-pixel basis. Finally, the values were totaled to obtain total parameter values including mean K_{trans} and V_p values from all of the segmented areas (Figure 3).

The data acquired from each section were summed to derive the voxel-by-voxel perfusion maps for the entire total VOI extent of the

image using the software NordicICE. Histograms of K_{trans} and V_p were plotted with each corresponding value on the x-axis, with a bin size of 0.5, while the y-axis measured the total number of pixels. For further quantitative analysis, cumulative histograms were obtained from the previous histograms. In the cumulative histograms, the cumulative number of observations in all bins up to the specified bin was mapped on the y-axis as a percentage. The mean values were derived from the K_{trans} and V_p histograms.(28)

Statistical analysis

Statistical analyses were performed using the Statistical Package for the Social Sciences version 21.0 (SPSS; Chicago, IL, USA) and the R statistical programming environment version 3.0.2. (the R Foundation, Vienna, Austria). All perfusion parameter data were collected and arranged into datasets according to patient group (migraine vs control) and brain region. The Kolmogorov-Smirnov test was applied to all datasets to determine whether they had a normal distribution. Perfusion parameter datasets from the alleged migraine-associated brain regions in the migraine group and from

the same region in the control group were compared to each other one by one. For comparison between two groups, the unpaired t-test or Mann-Whitney test was used. For clinical characteristics, the unpaired t-test or Mann-Whitney test was used between two frequency-based subgroups. Receiver operating characteristic curve analysis and logistic regression analysis were used to identify correlations between clinical characteristics and the aforementioned perfusion parameters and their cutoff values. *P*-values lower than 0.05 were considered significant.

Results

Patient characteristics

Clinical characteristics in 35 migraine patients are summarized in Table 1. They included age; sex; duration of migraine; characteristics of headache attack, including frequency, laterality, and intensity; symptoms accompanying the headache attack (visual symptoms such as scotomas, shimmering spots, changes in vision, vision loss, and flashing lights; motor–sensory disturbances such as numbness, difficulty with speech, and paralysis or localized weakness; auditory and vestibular symptoms such as chronic dizziness, ear pressure, and auditory hallucination or delusion; gastrointestinal symptoms such as nausea, bloating, and vomiting; and mood symptoms such as depression, irritability, and fatigue); presence of aura; characteristics of aura (visual symptoms such as scotomas, vision loss, and flashing lights; motor–sensory disturbances such as numbness, difficulty with speech, and paralysis or localized weakness; auditory hallucination); and the presence of medication for migraine. The 56 participants were classified into two groups according to diagnosis of migraine;

35 migraine patients assigned to the migraine group and 21 control subjects to the control group. The mean age of the migraine group was 57.23 ± 12.43 years (range, 26 – 79 years) and that of the control group was 71.33 ± 7.85 years (range, 58 – 87 years). The mean age in the migraine group was significantly younger than that in the control group (p <0.0001).

Among the 35 migraine patients, each patient had suffered from episodic migraines for at least one year. No clinical characteristics showed a significant difference between the LF and HF subgroups (Table 1).

The migraine attack laterality in the migraine group was as follows: 17.14% (6/35) experienced mainly on the right side, 25.71% (9/35) mainly on the left side, and 57.14% (20/35) on bilateral sides.

Comparison of DCE PK parameters: migraine versus control

Based on the result of the comparison analysis regarding the K_{trans} and V_p values between migraine and control groups (Supplementary

Table 3), the mean value of V_p in the left amygdala was decreased in the migraine group (p=0.0382) (Table 2, Figure 4).

Correlation between quantitative imaging parameters and clinical characteristics in migraine patients

The 35 migraine patients were stratified by the mean value of V_p in the left amygdala by using the highest value of the area under the receiver operating characteristic curve (0.711, 95% confidence interval, 0.5330 – 0.8510, p=0.0208), with which the cutoff value for classification was 0.2931 ml/100mg. The cutoff value of 0.2931 ml/100mg exhibited a prediction rate of 78.57% (11/14) and 61.90% (13/21) for the intensity of headache attack in the two subgroups of migraine patients, respectively. The mean value of V_p in the left amygdala had a correlation with only the intensity of headache attack in migraine patients (p=0.0350), and other clinical variables showed no significant correlation with the mean value of V_p in the left amygdala (p>0.05): frequency of migraine attack (p>0.05); bilateral versus unilateral location migraine attack (p>0.05) and right or left sided predominance in case of unilaterality (p>0.05); intensity of

headache attack (p>0.05); the presence of aura or accompanying symptom during headache (p>0.05); and status of medication (p>0.05).

Discussion

In our study, the mean value of V_p in the left amygdala from DCE MRI demonstrated a significant difference between the migraine and control groups (Table 2). Thus, patients with migraine exhibited increased permeability and a subsequent reduction in local blood plasma volume fraction in alleged migraine-associated regions compared with control subjects. In addition, the mean value of V_p in the left amygdala showed a significant correlation with the intensity of headache attack in migraine patients. Therefore, as these observations suggest that BBB impairment in migraine-associated brain regions including the amygdala can be related to pathophysiologic change in migraine patients, DCE MRI evaluation of BBB permeability has a clinical potential for diagnosis as well as a noninvasive imaging biomarker in migraine patients.

Few studies have used DCE MRI to quantify BBB permeability in migraine patients. Clinically, our study can provide quantitative imaging parameters in migraine-associated brain regions that show pathophysiologic mechanisms in migraine, such as the change in BBB

permeability. A few previous studies reported the involvement of those regions, including the left amygdala(6) in migraine. Pain perception, a complex process, may involve multiple interconnected brain regions for nociception(29), and the altered functional connectivity of pain network contributes to the pathophysiology of migraine. Based on prior functional MRI studies, migraine patients typically have reduced tolerance of visual, somatosensory, and auditory stimuli.(17) Recently, there have been lots of previous studies on the structural and functional changes of grey matter volume in migraine (17, 30). The structural changes, especially in the limbic regions may be associated with the repetitive pain processes and associated symptoms of migraine.(31) The volume of amygdala is negatively related to the frequency of headache attacks as a consequence of repeated brain insults during migraine attacks.(31) In addition to the structural changes, there are complex functional connectivities underlying the brain changes in migraine.(31) Among them, one of the main contributors to the neurolimbic pain network system, the amygdala, is involved in the modulation of synaptic transmission by cortical spreading depression and migraine

pain modulation.(32, 33) The enhanced functional connectivity of the left amygdala is observed in migraine, and this laterality may be associated with the different functions of each amygdala in that left amygdala contribute to the brain reward system.(33) The active amygdala-linked inhibitory control systems for pain reduction are associated with an increase in the pain experience.(34) The mean value of V_p in the left amygdala had a correlation with the visual analogue scale (VAS) intensity of headache attack in migraine patients. In spite of its subjectivity, the correlation between the VAS intensity of headache attack and the mean value of V_p in left amygdala may reflect one of the many aspects of the pain experience. Thus, increased BBB permeability as one of the pathophysiologic changes in migraine may contribute in the altered functional connectivity between those migraine-associated pain network regions. Further studies are required to determine how these permeability-related changes can be used for diagnosis, monitoring their progression, and evaluation of their effects.

As the tradeoff is a lower contrast-to-noise ratio in the first pass due to the low T1 relaxivity, which affects the precise

measurement of cerebral blood flow and volume, DCE MRI requires a compromise in terms of spatial resolution in weakly vascularized tissue.(10) To detect more subtle BBB permeability changes, a longer measurement is required to allow more contrast to enter the extravascular space. As slower leakage rates are important in chronic diseases such as Alzheimer's disease, lacunar stroke, (26) a short total sampling interval is inadequate for accurate measurement in migraine with slower leakage rates.(14, 15) As the chance of gross patient motion not correctable with motion-correcting algorithms would be inevitable in case of long-term measurement, however, relatively shorter time of measurement with respect to the slow leakage rates in migraine can be overcome by comparatively high T1 relaxivity of the gadobutrol used in this study.

This study has some potential limitations. First, we could not include age-matched controls in this study. The control group was composed of healthy subjects based on their clinical and imaging data. Despite of their age, they were free from cerebral microvascular disease, so the BBB permeability difference with normal aging was negligible. Even though the mean age of the migraine group was

significantly younger than that of the control group, the BBB permeability in migraine patients was increased over the control group. In consideration of age-related increased BBB permeability, the pathologically increased BBB permeability in migraine may be greater than the increased BBB permeability that occurs with normal aging in control subjects.(14) Second, we could not correlate the medication response in migraine patients with PK parameters in our study which also needs to be further addressed in clinical studies.

In conclusion, the decreased V_p in the left amygdala is related to migraine, which can be used as a migraine-associated imaging biomarker.

References

1. Olesen J, Steiner T. The International classification of headache disorders, 2nd edn (ICDH-II). BMJ Publishing Group Ltd; 2004.

2. Coppola G, Pierelli F, Schoenen J. Is the cerebral cortex hyperexcitable or hyperresponsive in migraine? Cephalalgia : an international journal of headache. 2007;27(12):1427-39.

3. Aurora S, Wilkinson F. The brain is hyperexcitable in migraine. Cephalalgia. 2007;27(12):1442-53.

4. May A. New insights into headache: an update on functional and structural imaging findings. Nature reviews Neurology. 2009;5(4):199-209.

5. Welch K, Nagesh V, Aurora SK, Gelman N. Periaqueductal gray matter dysfunction in migraine: cause or the burden of illness? Headache: The Journal of Head and Face Pain. 2001;41(7):629-37.

6. Hadjikhani N, Ward N, Boshyan J, Napadow V, Maeda Y, Truini A, et al. The missing link: enhanced functional connectivity between amygdala and visceroceptive cortex in migraine.

Cephalalgia : an international journal of headache. 2013;33(15):1264-8.

7. Moskowitz MA. Holes in the leaky migraine blood-brain barrier hypothesis? Brain. 2017;140(6):1537-9.

8. Noseda R, Burstein R. Migraine pathophysiology: anatomy of the trigeminovascular pathway and associated neurological symptoms, cortical spreading depression, sensitization, and modulation of pain. Pain. 2013;154 Suppl 1:S44-53.

9. Shi L, Wang D, Liu W, Fang K, Wang YXJ, Huang W, et al. Automatic detection of arterial input function in dynamic contrast enhanced MRI based on affinity propagation clustering. Journal of Magnetic Resonance Imaging. 2014;39(5):1327-37.

10. Sourbron SP, Buckley DL. Classic models for dynamic contrast-enhanced MRI. NMR in biomedicine. 2013;26(8):1004-27.

11. Larsson HB, Courivaud F, Rostrup E, Hansen AE. Measurement of brain perfusion, blood volume, and blood-brain barrier permeability, using dynamic contrast-enhanced T(1)-weighted MRI at 3 tesla. Magnetic resonance in medicine. 2009;62(5):1270-81.

12. DosSantos MF, Holanda-Afonso RC, Lima RL, DaSilva AF, Moura-Neto V. The role of the blood-brain barrier in the development and treatment of migraine and other pain disorders. Frontiers in cellular neuroscience. 2014;8:302.

13. Zlokovic BV. The blood-brain barrier in health and chronic neurodegenerative disorders. Neuron. 2008;57(2):178-201.

14. Farrall AJ, Wardlaw JM. Blood-brain barrier: ageing and microvascular disease--systematic review and meta-analysis. Neurobiology of aging. 2009;30(3):337-52.

15. Taheri S, Gasparovic C, Shah NJ, Rosenberg GA. Quantitative measurement of blood-brain barrier permeability in human using dynamic contrast-enhanced MRI with fast T1 mapping. Magnetic resonance in medicine. 2011;65(4):1036-42.

16. Ewing JR, Brown SL, Lu M, Panda S, Ding G, Knight RA, et al. Model selection in magnetic resonance imaging measurements of vascular permeability: Gadomer in a 9L model of rat cerebral tumor. Journal of cerebral blood flow and metabolism : official journal of the International Society of Cerebral Blood Flow and Metabolism. 2006;26(3):310-20.

17. Maleki N, Becerra L, Brawn J, Bigal M, Burstein R, Borsook D. Concurrent functional and structural cortical alterations in migraine. Cephalalgia : an international journal of headache. 2012;32(8):607-20.

18. Khan AR, Wang L, Beg MF. FreeSurfer-initiated fully-automated subcortical brain segmentation in MRI using Large Deformation Diffeomorphic Metric Mapping. NeuroImage. 2008;41(3):735-46.

19. Reuter M, Tisdall MD, Qureshi A, Buckner RL, van der Kouwe AJ, Fischl B. Head motion during MRI acquisition reduces gray matter volume and thickness estimates. NeuroImage. 2015;107:107-15.

20. Sled JG, Zijdenbos AP, Evans AC. A nonparametric method for automatic correction of intensity nonuniformity in MRI data. IEEE transactions on medical imaging. 1998;17(1):87-97.

21. Segonne F, Pacheco J, Fischl B. Geometrically accurate topology-correction of cortical surfaces using nonseparating loops. IEEE transactions on medical imaging. 2007;26(4):518-29.

22. Fischl B, Dale AM. Measuring the thickness of the human cerebral cortex from magnetic resonance images. Proceedings of the

National Academy of Sciences of the United States of America. 2000;97(20):11050-5.

23. Nam J, Kang K, Choi S, Lim W, Yoo R-E, Kim J-H, et al. Comparison between the Prebolus T1 Measurement and the Fixed T1 Value in Dynamic Contrast-Enhanced MR Imaging for the Differentiation of True Progression from Pseudoprogression in Glioblastoma Treated with Concurrent Radiation Therapy and Temozolomide Chemotherapy. American Journal of Neuroradiology. 2017;38(12):2243-50.

24. Butman J, Gupta S, editors. Automated computation of the vascular input function for dynamic contrast-enhanced MRI of the brain. Abstract 14th Scientific Meeting, ISMRM; 2006.

25. Kamson DO, Illés Z, Aradi M, Orsi G, Perlaki G, Leél-Őssy E, et al. Volumetric comparisons of supratentorial white matter hyperintensities on FLAIR MRI in patients with migraine and multiple sclerosis. Journal of Clinical Neuroscience. 2012;19(5):696-701.

26. van de Haar HJ, Burgmans S, Jansen JF, van Osch MJ, van Buchem MA, Muller M, et al. Blood-Brain Barrier Leakage in Patients with Early Alzheimer Disease. Radiology. 2016;281(2):527-35.

27. Bergamino M, Bonzano L, Levrero F, Mancardi G, Roccatagliata L. A review of technical aspects of T 1−weighted dynamic contrast−enhanced magnetic resonance imaging (DCE−MRI) in human brain tumors. Physica Medica. 2014;30(6):635−43.

28. Jung SC, Choi SH, Yeom JA, Kim J−H, Ryoo I, Kim SC, et al. Cerebral blood volume analysis in glioblastomas using dynamic susceptibility contrast−enhanced perfusion MRI: a comparison of manual and semiautomatic segmentation methods. PloS one. 2013;8(8):e69323.

29. Peyron R, Laurent B, Garcia−Larrea L. Functional imaging of brain responses to pain. A review and meta−analysis (2000). Neurophysiologie clinique = Clinical neurophysiology. 2000;30(5):263−88.

30. Jin C, Yuan K, Zhao L, Zhao L, Yu D, von Deneen KM, et al. Structural and functional abnormalities in migraine patients without aura. NMR in biomedicine. 2013;26(1):58−64.

31. Jia Z, Yu S. Grey matter alterations in migraine: A systematic review and meta−analysis. NeuroImage Clinical. 2017;14:130−40.

32. Dehbandi S, Speckmann EJ, Pape HC, Gorji A. Cortical

spreading depression modulates synaptic transmission of the rat lateral amygdala. The European journal of neuroscience. 2008;27(8):2057-65.

33. Chen Z, Chen X, Liu M, Dong Z, Ma L, Yu S. Altered functional connectivity of amygdala underlying the neuromechanism of migraine pathogenesis. The journal of headache and pain. 2017;18(1):7.

34. Schwedt TJ, Schlaggar BL, Mar S, Nolan T, Coalson RS, Nardos B, et al. Atypical resting-state functional connectivity of affective pain regions in chronic migraine. Headache. 2013;53(5):737-51.

Tables

Table 1. Clinical characteristics in 35 migraine patients between low-frequency and high-frequency subgroups

	Subgroup				
	Low-frequency		High-frequency		*p*-value
Total patients (Male : Female)	24 (5 : 19)		11 (4 : 7)		0.3565
Mean age (years)	56.46 ± 12.70 (26 - 79)		58.91 ± 12.22 (33 - 77)		0.5956
Duration of migraine (years)	12.17 ± 13.44 (1 - 41)		20.09 ± 16.83 (2 - 48)		0.0639
Headache characteristics					
Laterality	Bilateral sided	41.67% (10/24)	Bilateral sided	90.91% (10/11)	

	Right sided	25.00% (6/24)	Right sided	0.00% (0/11)	
	Left sided	33.33% (8/24)	Left sided	9.09% (1/11)	
Intensity (VAS 1−10)	4.55 ± 2.40 (2 – 10)		5.75 ± 2.73 (1 – 10)		0.1476
Associated symptoms along with headache					
Visual symptoms	45.83% (11/24)		54.55% (6/11)		0.6370
Motor−sensory disturbance	8.33% (2/24)		9.09% (1/11)		1.0000
Auditory and vestibular symptoms	25.00% (6/24)		36.36% (4/11)		0.4959
Gastrointestinal symptoms	66.67% (16/24)		45.45% (5/11)		0.2412
Mood symptoms	41.67% (10/24)		45.45% (5/11)		0.8359
Aura					
Presence of aura	58.33% (14/24)		63.64% (7/11)		0.7695

Characteristics of aura			
Visual symptoms	4.17% (1/24)	18.18% (2/11)	0.2269
Motor-sensory disturbance	0.00% (0/24)	9.09% (1/11)	0.3143
Auditory symptoms	8.33% (2/24)	18.18% (2/11)	0.5748
Medication	70.83% (17/24)	72.73% (8/11)	0.9096

Note: VAS = visual analog scale

Table 2. Significant imaging parameter from results of comparison analyses of the K_{trans} and V_p values according to automatic segmented masks in bilateral, right, and left hemispheres between migraine and control groups.

		Group		
Imaging parameters	Region of interest	Migraine	Control	*p*−value
$V_{p\ mean}$	Left amygdala	$4.45x10^{-1} \pm 4.64x10^{-1}$	$7.17x10^{-1} \pm 9.22x10^{-1}$	0.0382

Figure legends

Figure 1. Flowchart for selecting the study population

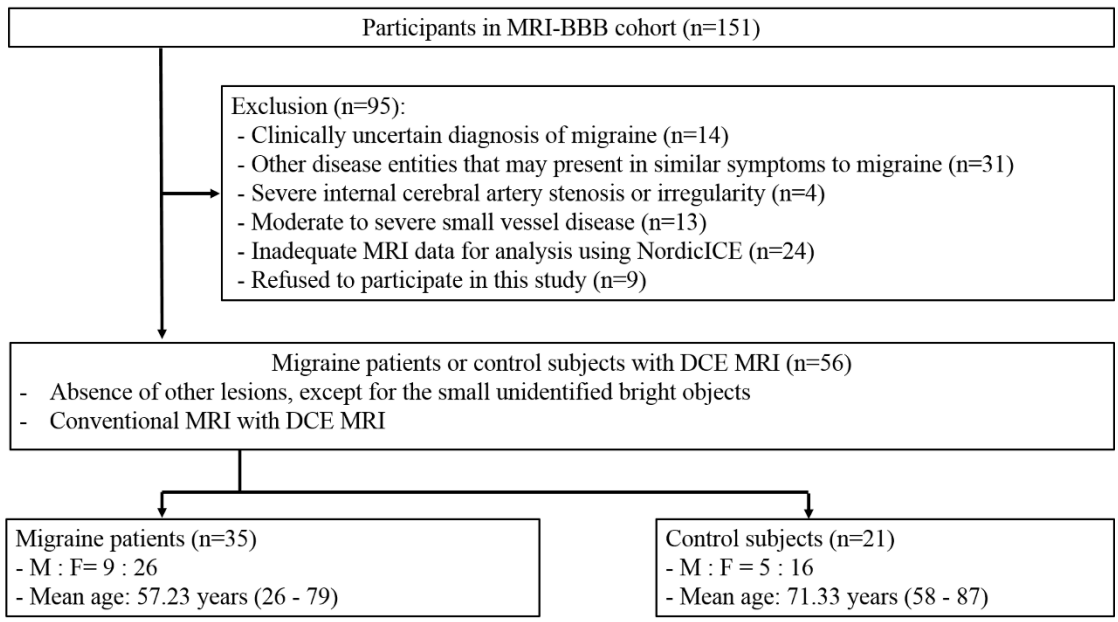

Figure 2. Flow diagram of the automatic cortical reconstruction and volumetric segmentation

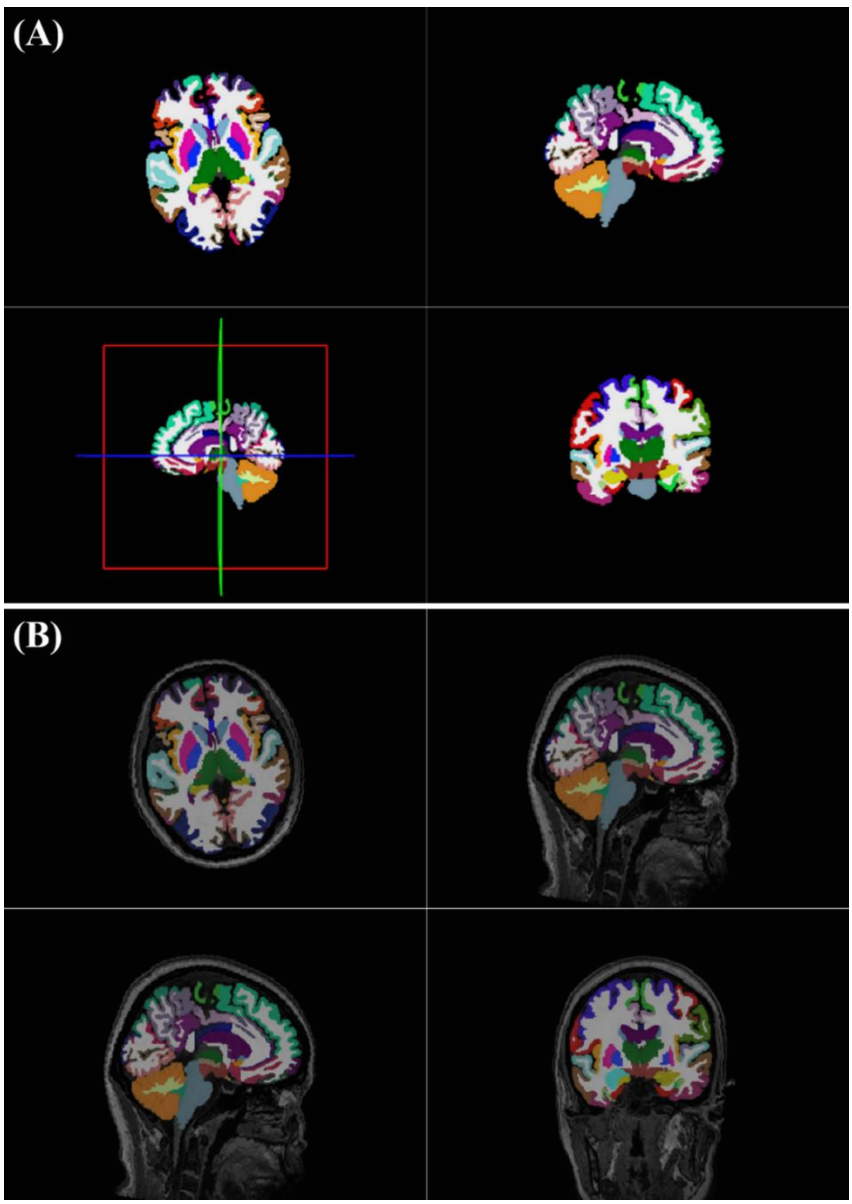

Figure 2-(A). Color maps load all the volumes of different brain regions and their own associated colors including axial, sagittal, coronal, and 3D (clockwise). The opacity can be adjusted between 0, completely transparent, and 1, completely opaque.

Figure 2-(B). Regions of interest can be adjusted visually according to region-associated colors. The brain regions of interest in conventional MRI can be presented as overlaid colored masks with the opacity value of 0.5 in the color map.

Figure 3. Flow diagram of the perfusion analysis and coregistration between perfusion maps and region of interest masks

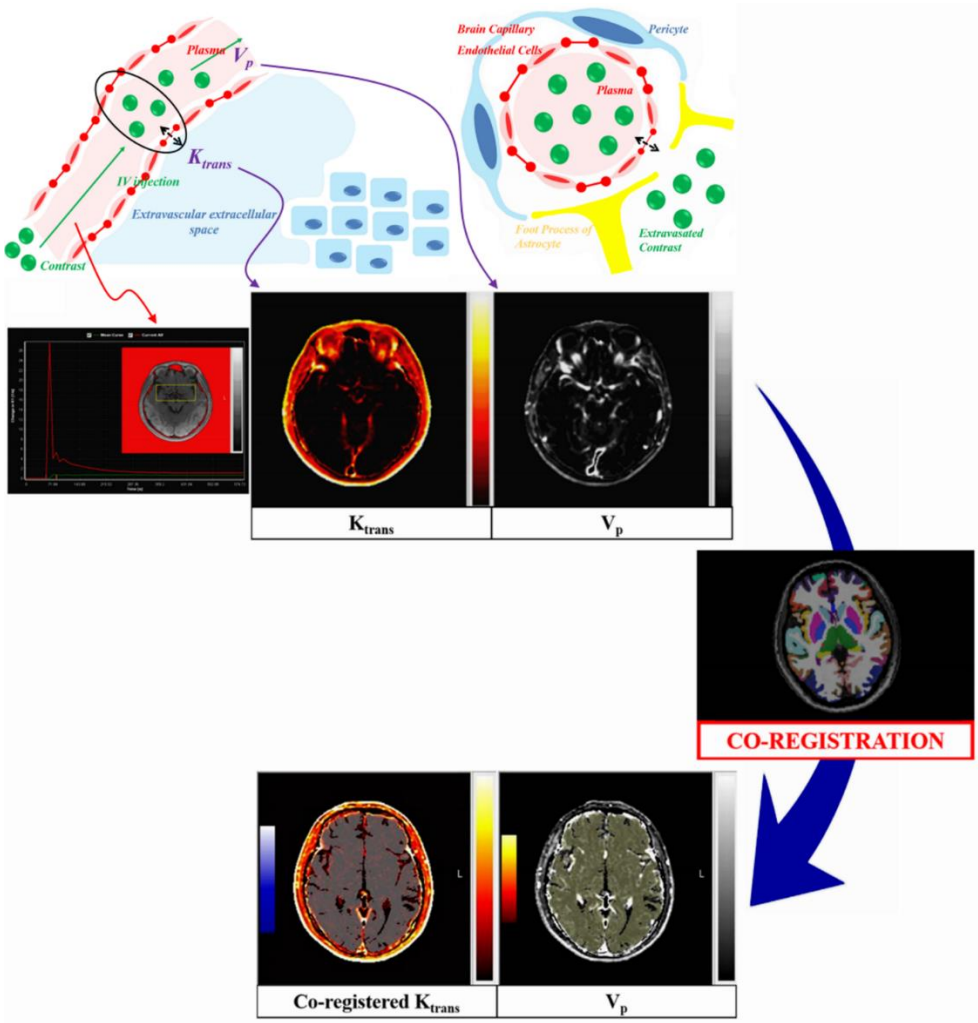

Schematic illustration of the measurement of blood-brain barrier (BBB) disruption using dynamic contrast-enhanced (DCE) magnetic resonance (MR) imaging. The BBB is formed by brain capillary

endothelial cells (double pink ovals) sealed by tight junctions (red dumbbells), pericytes (double sky-blue ovals with extending edges) and foot processes of astrocytes (yellow triangles). After low-molecular-weight magnetic resonance imaging contrast agent (green circles) administration, BBB disruption (dotted black arrow) can enable the contrast extravasation and its accumulation in the extravascular extracellular space. The volume transfer constant K_{trans} represents the rate at which contrast agent is delivered to the extravascular extracellular space per volume of tissue, and the fractional plasma volume V_p represents blood plasma volume per unit volume of tissue.

Automatically extracted arterial input function (AIF) graph (red graph) and its AIF-derived PK parameters: K_{trans} and V_p maps. The yellow box represents searching boxes at the level of the middle cerebral artery horizontal segment for the AIF. After coregistration between perfusion maps and automatically segmented brain region masks, the total volumes of interest were determined.

Figure 4. A box-whisker plot of V_p in left amygdala for migraine and control groups.

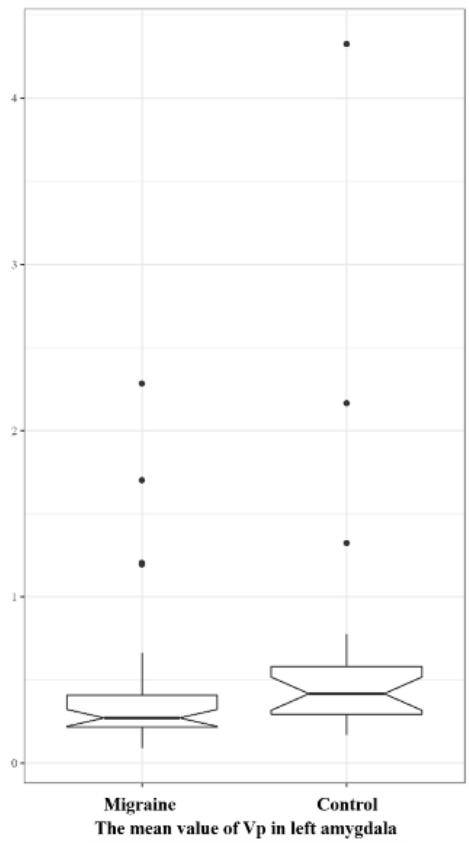

A box-whisker plot of V_p in the left amygdala is shown for two groups (migraine patients vs control subjects). Notched lines of boxes = median values. Boundaries of boxes = 25^{th} and 75^{th} percentiles, with whiskers extending from the median to ± 1.5 x interquartile ranges and outliers beyond the whiskers denoted by

points.

Supplementary tables

Supplementary Table 1. Magnetic resonance scan parameters

Machine	Discovery 750		
Field strength (T)	3.0		
Head coil channel	32		
Imaging sequence	DCE-MRI	preT1 and postT1	FLAIR
Repetition time (ms)	3.0	8.5	7200
Echo time (ms)	1.1	3.2	113.8

Flip angle (°)	10	12	90
Number of excitation	0.7	1	1
Matrix	128 x 128	256 x 230	256 x 230
Section thickness (mm)	3	1	1
Intersection gap (mm)	1.5	0	0
Field of view (mm)	249 x 249	256 x 256	256 x 256
Phase	60		
Scan time for 1 phase (sec)	5		
Total scan time (sec)	5 min 25 sec		

NOTE: DCE-MRI = dynamic contrast-enhanced magnetic resonance imaging; preT1=pre-contrast T1 weighted image; postT1=post-contrast enhanced T1 weighted image; FLAIR=fluid attenuated inversion recovery

Supplementary Table 2. Brain regions of interest related to the migraine

Category	Brain regions
Cortex	Postcentral gyrus
	Cingulate gyrus
	Insula
	Parahippocampal gyrus
	Pericalcarine gyrus
Deep brain structure	Thalamus
	Basal ganglia [a]
	Nucleus accumbens
	Caudate
	Putamen
	Pallidum

	Substantia nigra
Pain modulatory systems	Hippocampus
	Amygdala
	Brainstem
White matter	White matter of cerebral hemisphere

NOTE: [a] Basal ganglia are composed of nucleus accumbens, caudate, putamen, pallidum, and subthalamic nucleus.

Supplementary Table 3. Imaging parameters from the representative results of comparison analyses for the K_{trans} and V_p mean values according to automatic segmented masks between migraine and control groups

			Group		
Imaging parameter	Laterality	Interested location	Migraine	Control	*p*-value
$K_{trans\ mean}$ (ml/100g/min)	Bilateral	Postcentral gyrus	$3.00x10^{-4}\pm2.60x10^{-4}$	$6.10x10^{-4}\pm7.10x10^{-4}$	0.2750
		Cingulate gyrus	$5.00x10^{-4}\pm4.70x10^{-4}$	$7.00x10^{-4}\pm8.00x10^{-4}$	0.8590
		Insula	$3.60x10^{-4}\pm3.70x10^{-4}$	$4.00x10^{-4}\pm4.50x10^{-4}$	0.7034
		Parahippocampal gyrus	$14.10x10^{-4}\pm14.30x10^{-4}$	$16.20x10^{-4}\pm22.70x10^{-4}$	0.3563

		Pericalcarine gyrus	$2.80x10^{-4}\pm2.40x10^{-4}$	$4.10x10^{-4}\pm4.70x10^{-4}$	0.3563
		Thalamus	$2.80x10^{-4}\pm2.60x10^{-4}$	$3.40x10^{-4}\pm3.50x10^{-4}$	0.8061
		Basal ganglia	$2.50x10^{-4}\pm2.50x10^{-4}$	$3.20x10^{-4}\pm3.50x10^{-4}$	0.7931
		Nucleus accumbens	$3.10x10^{-4}\pm3.20x10^{-4}$	$3.70x10^{-4}\pm3.60x10^{-4}$	0.7931
		Caudate	$2.70x10^{-4}\pm2.60x10^{-4}$	$3.90x10^{-4}\pm5.00x10^{-4}$	0.8990
		Putamen	$2.40x10^{-4}\pm2.50x10^{-4}$	$2.80x10^{-4}\pm2.90x10^{-4}$	0.8193
		Pallidum	$2.30x10^{-4}\pm2.20x10^{-4}$	$2.70x10^{-4}\pm2.70x10^{-4}$	0.9663
		Substantia nigra	$3.70x10^{-4}\pm3.80x10^{-4}$	$4.50x10^{-4}\pm6.10x10^{-4}$	0.9932
		Hippocampus	$3.90x10^{-4}\pm3.80x10^{-4}$	$5.60x10^{-4}\pm8.60x10^{-4}$	0.8590

		Amygdala	$3.70x10^{-4}\pm4.00x10^{-4}$	$4.00x10^{-4}\pm4.50x10^{-4}$	0.9595
		Brainstem	$2.90x10^{-4}\pm2.80x10^{-4}$	$5.30x10^{-4}\pm10.40x10^{-4}$	0.6057
		WM of cerebral hemisphere	$1.90x10^{-4}\pm1.80x10^{-4}$	$3.10x10^{-4}\pm3.30x10^{-4}$	0.2863
	Right	Postcentral gyrus	$2.90x10^{-4}\pm2.50x10^{-4}$	$5.90x10^{-4}\pm7.40x10^{-4}$	0.3305
		Cingulate gyrus	$6.00x10^{-4}\pm7.20x10^{-4}$	$7.90x10^{-4}\pm11.50x10^{-4}$	0.8856
		Insula	$3.60x10^{-4}\pm3.70x10^{-4}$	$4.00x10^{-4}\pm4.40x10^{-4}$	0.8723
		Parahippocampal gyrus	$15.40x10^{-4}\pm15.2x10^{-4}$	$18.40x10^{-4}\pm27.70x10^{-4}$	0.3390
		Pericalcarine gyrus	$3.10x10^{-4}\pm2.60x10^{-4}$	$4.70x10^{-4}\pm4.80x10^{-4}$	0.6057

		Thalamus	$2.90x10^{-4}\pm2.70x10^{-4}$	$3.70x10^{-4}\pm3.70x10^{-4}$	0.8590
		Basal ganglia	$2.60x10^{-4}\pm2.50x10^{-4}$	$3.20x10^{-4}\pm3.50x10^{-4}$	0.9258
		Nucleus accumbens	$3.20x10^{-4}\pm3.50x10^{-4}$	$3.60x10^{-4}\pm3.30x10^{-4}$	0.5707
		Caudate	$2.90x10^{-4}\pm2.60x10^{-4}$	$3.90x10^{-4}\pm5.30x10^{-4}$	0.8061
		Putamen	$2.50x10^{-4}\pm2.60x10^{-4}$	$2.80x10^{-4}\pm2.80x10^{-4}$	0.9528
		Pallidum	$2.30x10^{-4}\pm2.10x10^{-4}$	$2.70x10^{-4}\pm2.70x10^{-4}$	0.8590
		Substantia nigra	$3.70x10^{-4}\pm3.90x10^{-4}$	$4.50x10^{-4}\pm6.40x10^{-4}$	0.8990
		Hippocampus	$4.00x10^{-4}\pm3.80x10^{-4}$	$7.30x10^{-4}\pm15.60x10^{-4}$	0.9528
		Amygdala	$3.70x10^{-4}\pm3.80x10^{-4}$	$4.50x10^{-4}\pm5.40x10^{-4}$	0.9191

		WM of cerebral hemisphere	$2.00x10^{-4}\pm1.80x10^{-4}$	$3.20x10^{-4}\pm3.50x10^{-4}$	0.1896
	Left	Postcentral gyrus	$3.10x10^{-4}\pm2.80x10^{-4}$	$6.30x10^{-4}\pm6.80x10^{-4}$	0.4514
		Cingulate gyrus	$4.10x10^{-4}\pm3.70x10^{-4}$	$6.80x10^{-4}\pm7.80x10^{-4}$	0.3652
		Insula	$3.70x10^{-4}\pm3.80x10^{-4}$	$4.10x10^{-4}\pm4.60x10^{-4}$	0.7414
		Parahippocampal gyrus	$13.10x10^{-4}\pm13.90x10^{-4}$	$14.6x10^{-4}\pm20.10x10^{-4}$	0.4313
		Pericalcarine gyrus	$2.60x10^{-4}\pm2.30x10^{-4}$	$3.60x10^{-4}\pm4.90x10^{-4}$	0.7160
		Thalamus	$2.60x10^{-4}\pm2.60x10^{-4}$	$3.30x10^{-4}\pm3.40x10^{-4}$	0.7414
		Basal ganglia	$2.40x10^{-4}\pm2.40x10^{-4}$	$3.20x10^{-4}\pm3.90x10^{-4}$	0.7671

		Nucleus accumbens	$3.10x10^{-4}\pm3.00x10^{-4}$	$3.80x10^{-4}\pm4.60x10^{-4}$	0.8457
		Caudate	$2.60x10^{-4}\pm2.60x10^{-4}$	$3.80x10^{-4}\pm5.50x10^{-4}$	0.7801
		Putamen	$2.30x10^{-4}\pm2.30x10^{-4}$	$2.80x10^{-4}\pm3.10x10^{-4}$	0.7160
		Pallidum	$2.30x10^{-4}\pm2.30x10^{-4}$	$2.60x10^{-4}\pm2.70x10^{-4}$	0.8656
		Substantia nigra	$3.60x10^{-4}\pm3.80x10^{-4}$	$4.50x10^{-4}\pm6.00x10^{-4}$	0.9797
		Hippocampus	$3.80x10^{-4}\pm3.90x10^{-4}$	$4.40x10^{-4}\pm4.70x10^{-4}$	0.8061
		Amygdala	$3.60x10^{-4}\pm4.10x10^{-4}$	$3.60x10^{-4}\pm3.5x10^{-4}$	0.8061
		WM of cerebral hemisphere	$1.90x10^{-4}\pm1.70x10^{-4}$	$3.00x10^{-4}\pm3.20x10^{-4}$	0.3221
$V_{p\ mean}$	Bilateral	Postcentral gyrus	$5.39x10^{-1}\pm5.01x10^{-1}$	$7.30x10^{-1}\pm6.77x10^{-1}$	0.2676

(ml/100g)		Cingulate gyrus	$8.60x10^{-1}\pm8.82x10^{-1}$	$10.89x10^{-1}\pm13.27x10^{-1}$	0.6784
		Insula	$8.66x10^{-1}\pm8.91x10^{-1}$	$10.08x10^{-1}\pm12.16x10^{-1}$	0.6661
		Parahippocampal gyrus	$13.67x10^{-1}\pm14.23x10^{-1}$	$15.89x10^{-1}\pm19.56x10^{-1}$	0.8325
		Pericalcarine gyrus	$7.20x10^{-1}\pm6.97x10^{-1}$	$8.92x10^{-1}\pm9.47x10^{-1}$	0.6296
		Thalamus	$5.18x10^{-1}\pm4.95x10^{-1}$	$7.54x10^{-1}\pm6.99x10^{-1}$	0.1896
		Basal ganglia	$4.42x10^{-1}\pm4.33x10^{-1}$	$5.37x10^{-1}\pm5.71x10^{-1}$	0.7414
		Nucleus accumbens	$4.83x10^{-1}\pm4.77x10^{-1}$	$6.03x10^{-1}\pm6.36x10^{-1}$	0.4616
		Caudate	$4.80x10^{-1}\pm4.61x10^{-1}$	$5.85x10^{-1}\pm6.25x10^{-1}$	0.8723

		Putamen	$4.60x10^{-1}\pm4.53x10^{-1}$	$5.63x10^{-1}\pm6.15x10^{-1}$	0.6908
		Pallidum	$3.30x10^{-1}\pm3.26x10^{-1}$	$4.21x10^{-1}\pm4.31x10^{-1}$	0.4313
		Substantia nigra	$7.88x10^{-1}\pm7.36x10^{-1}$	$9.77x10^{-1}\pm13.67x10^{-1}$	0.3563
		Hippocampus	$8.51x10^{-1}\pm9.25x10^{-1}$	$11.37x10^{-1}\pm11.47x10^{-1}$	0.2604
		Amygdala	$4.82x10^{-1}\pm4.93x10^{-1}$	$6.50x10^{-1}\pm5.98x10^{-1}$	0.2750
		Brainstem	$4.30x10^{-1}\pm4.07x10^{-1}$	$7.69x10^{-1}\pm10.85x10^{-1}$	0.1298
		WM of cerebral hemisphere	$2.70x10^{-1}\pm2.50x10^{-1}$	$4.23x10^{-1}\pm4.40x10^{-1}$	0.1215
	Right	Postcentral gyrus	$5.55x10^{-1}\pm5.12x10^{-1}$	$7.58x10^{-1}\pm7.59x10^{-1}$	0.3139
		Cingulate gyrus	$11.01x10^{-1}\pm14.31x10^{-1}$	$11.25x10^{-1}\pm13.11x10^{-1}$	0.6908
		Insula	$8.20x10^{-1}\pm8.08x10^{-1}$	$10.19x10^{-1}\pm12.69x10^{-1}$	0.8457

		Parahippocampal gyrus	$15.36x10^{-1}\pm16.29x10^{-1}$	$18.15x10^{-1}\pm23.77x10^{-1}$	0.8457
		Pericalcarine gyrus	$8.17x10^{-1}\pm8.18x10^{-1}$	$9.88x10^{-1}\pm10.78x10^{-1}$	0.6176
		Thalamus	$5.84x10^{-1}\pm5.81x10^{-1}$	$8.25x10^{-1}\pm7.57x10^{-1}$	0.4514
		Basal ganglia	$4.65x10^{-1}\pm4.63x10^{-1}$	$5.50x10^{-1}\pm5.77x10^{-1}$	0.7801
		Nucleus accumbens	$4.93x10^{-1}\pm4.94x10^{-1}$	$6.31x10^{-1}\pm6.96x10^{-1}$	0.7542
		Caudate	$5.16x10^{-1}\pm5.13x10^{-1}$	$6.21x10^{-1}\pm6.81x10^{-1}$	0.8990
		Putamen	$4.84x10^{-1}\pm4.79x10^{-1}$	$5.75x10^{-1}\pm6.21x10^{-1}$	0.6296
		Pallidum	$3.36x10^{-1}\pm3.43x10^{-1}$	$4.34x10^{-1}\pm4.53x10^{-1}$	0.3059

		Substantia nigra	$7.82x10^{-1}\pm7.17x10^{-1}$	$10.32x10^{-1}\pm14.89x10^{-1}$	0.5823
		Hippocampus	$9.07x10^{-1}\pm9.85x10^{-1}$	$11.89x10^{-1}\pm11.24x10^{-1}$	0.2825
		Amygdala	$5.33x10^{-1}\pm5.49x10^{-1}$	$6.45x10^{-1}\pm6.48x10^{-1}$	0.5707
		WM of cerebral hemisphere	$3.01x10^{-1}\pm2.80x10^{-1}$	$4.40x10^{-1}\pm4.74x10^{-1}$	0.1626
	Left	Postcentral gyrus	$5.27x10^{-1}\pm4.93x10^{-1}$	$7.17x10^{-1}\pm6.46x10^{-1}$	0.4616
		Cingulate gyrus	$7.09x10^{-1}\pm7.16x10^{-1}$	$10.64x10^{-1}\pm11.39x10^{-1}$	0.4022
		Insula	$9.25x10^{-1}\pm10.44x10^{-1}$	$10.06x10^{-1}\pm11.81x10^{-1}$	0.5367
		Parahippocampal gyrus	$12.39x10^{-1}\pm13.07x10^{-1}$	$14.34x10^{-1}\pm17.24x10^{-1}$	0.7542

		Pericalcarine gyrus	$6.33x10^{-1}\pm6.04x10^{-1}$	$8.32x10^{-1}\pm8.76x10^{-1}$	0.6057
		Thalamus	$4.73x10^{-1}\pm4.43x10^{-1}$	$7.13x10^{-1}\pm6.82x10^{-1}$	0.1626
		Basal ganglia	$4.23x10^{-1}\pm4.05x10^{-1}$	$5.26x10^{-1}\pm5.69x10^{-1}$	0.7801
		Nucleus accumbens	$4.82x10^{-1}\pm4.68x10^{-1}$	$5.82x10^{-1}\pm5.95x10^{-1}$	0.2533
		Caudate	$4.55x10^{-1}\pm4.32x10^{-1}$	$5.72x10^{-1}\pm6.18x10^{-1}$	0.7542
		Putamen	$4.40x10^{-1}\pm4.27x10^{-1}$	$5.54x10^{-1}\pm6.11x10^{-1}$	0.7034
		Pallidum	$3.24x10^{-1}\pm3.11x10^{-1}$	$4.11x10^{-1}\pm4.12x10^{-1}$	0.4022
		Substantia nigra	$7.89x10^{-1}\pm7.11x10^{-1}$	$9.38x10^{-1}\pm12.61x10^{-1}$	0.3743
		Hippocampus	$7.94x10^{-1}\pm8.58x10^{-1}$	$10.95x10^{-1}\pm12.86x10^{-1}$	0.2463

		Amygdala	$4.45x10^{-1}\pm4.64x10^{-1}$	$7.17x10^{-1}\pm9.22x10^{-1}$	0.0382 [a]
		WM of cerebral hemisphere	$2.60x10^{-1}\pm2.38x10^{-1}$	$4.07x10^{-1}\pm4.10x10^{-1}$	0.1256

NOTE: [a] statistically significant difference; WM = white matter

초 록

배경 및 목적: 본 연구에서는 동적 조영 증강 자기 공명 영상을 이용하여 편두통과 관련된 뇌 영역의 정량적 혈액 뇌 장벽 투과성을 측정하고, 편두통의 병태생리학적 위치를 결정하고자 한다.

재료 및 방법: 실제 임상 결과를 분석하기 위해 2016년 9월부터 2017년 12월에 걸쳐 가도뷰트롤 투여 후 얻은 동적 조영 증강 자기 공명 영상을 촬영한 56명의 피험자를 편두통군 (총 35명) 과 대조군 (총 21명)으로 분류하여 분석하였다. 프리서퍼를 사용하여 조영증강 전 T1 강조 영상에서 전체 뇌 영역에 대하여 자동 영역 분할을 수행하였다. 이후, 노르딕아이스를 사용하여 자동 영역 분할이 끝난 전체 뇌영역으로부터 편두통과 관련된 뇌 영역 마스크를 추출하였다. 동적 조영 증강 자기 공명 영상으로부터 혈관 내 영역에서 혈관외 세포외 공간 영역으로 이동되는 조영제의 분율을 표현한 체적전달상수 (K_{trans}) 지도와 혈관내 혈장 부피를 표현한 혈장체적지도 (V_p)를 추출하였다. 앞서 추출한 편두통과 관련된 뇌 영역 마스크마다 관류 관련 인자인 체적전달상수 (K_{trans}) 및 혈장체적 (V_p) 을 모두 구하고 그 영역 마스크에서 각 관류 관련 인자의 평균값을 구하였다. 편두통군과 대조군간에 각 관심 영역 마스크의 관류 관련 인자의 평균값을 비교하기 위해 독립표본티검정과 맨-휘트니

검정을 사용하였다. 수신자 조작 특성 곡선 분석과 로지스틱 회귀 분석을 이용하여 편두통 환자의 임상적 특성과 이전 비교 분석시 의미가 있었던 관류 관련 인자 간의 상관 관계를 확인하였다.

결과: 편두통군의 평균 연령은 57.23 세 (범위: 26 – 79세)로 대조군의 평균 연령 71.33 세 (범위: 58 – 87세)보다 유의하게 낮았다 ($P<0.0001$). 좌측 편도체에서 측정된 혈장체적 (V_p) 의 평균은 편두통군에서 $4.45x10^{-1}\pm4.64x10^{-1}$ ml/100g 이었고, 대조군에서 $7.17x10^{-1}\pm9.22x10^{-1}$ ml/100g 로 편두통군에서 유의하게 낮았다 ($P=0.0382$). 편두통 환자의 임상적 특성 중 두통 발작의 강도만이 좌측 편도체에서 측정된 혈장체적 (V_p) 의 평균값과 유의미한 상관관계가 있었다 ($P=0.0350$).

결론: 본 연구에서 좌측 편도체에서 혈장체적 (V_p) 평균의 감소는 편두통과 관련이 있었다. 해당 관류 관련 인자는 편두통과 연관된 위치에서 혈액 뇌 장벽의 증가된 투가도를 반영하는 영상 생체표지자로서 사용될 수 있을 것으로 생각된다.

주요어: 편두통, 동적 조영 증강 자기공명영상, 혈액 뇌 장벽, 투과도

학 번: 2017-27607